Figure 5 ^{7}Li NMR linewidth data as a function of temperature for P$_{12}$ doped with 9.3 mol% Li$^+$.

8. Hattori, M., Fukada, S., Nakamura, D. & Ikeda, R. Studies of the anisotropic self-diffusion and reorientation of butyl ammonium cations in the rotator phase of butyl ammonium chloride using ^{1}H magnetic resonance, electrical conductivity and thermal measurements. *J. Chem. Soc. Faraday Trans.* **86,** 3777–3783 (1990).
9. Ishida, H., Furukawa, Y., Kashino, S., Sato, S. & Ikeda, R. Phase transitions and ionic motions in solid trimethylethylammonium iodide studied by ^{1}H and [127]I NMR, electrical conductivity, X-ray diffraction and thermal analysis. *Ber. Bunsenges. Phys. Chem.* **100,** 433–439 (1996).
10. Tanabe, T., Nakamura, D. & Ikeda, R. Novel ionic plastic crystal phase of [(CH$_3$)$_4$N]SCN obtainable above 455K studied by proton magnetic resonance, electrical conductivity and thermal measurements. *J. Chem. Soc. Faraday Trans.* **87,** 987–990 (1991).
11. Shimizu, T., Tanaka, S., Onoda-Yamamuro, N., Ishimaru, S. & Ikeda, R. New rotator phase revealed in di-n-alkylammonium bromides studies by solid state NMR, powder XRD, electrical conductivity and thermal measurements. *J. Chem. Soc. Faraday Trans.* **93,** 321–326 (1997).
12. Cooper, E. I. & Angell, C. A. Ambient temperature plastic crystal fast ion conductors (PLICFICS). *Solid State Ionics* **18/19,** 570–576 (1986).
13. Aronson, R. *et al.* Fast ion conductors with rotating sulphate ions. *J. Phys. Colloq. C6* **41,** 35–37 (1980).
14. Aronson, R., Knape, H. E. G. & Torell, L. M. Brillouin spectra of the solid electrolyte Li$_2$SO$_4$. *J. Chem. Phys.* **77,** 677–680 (1982).
15. Borgesson, L. & Torell, L. M. Reorientational motion in superionic sulphates: A Raman linewidth study. *Phys. Rev. B* **32,** 2471–2477 (1985).
16. MacFarlane, D. R., Sun, J., Forsyth, M., Meakin, P. & Amini, N. Pyrrolidinium imides: a new family of molten salts and conductive plastic crystal phases. *J. Phys. Chem.* **103,** 4164–4170 (1999).
17. Sun, J., Forsyth, M. & MacFarlane, D. R. Room temperature molten salts based on the quarternary ammonium ion. *J. Phys. Chem.* **102,** 8858–8864 (1998).
18. Sylla, S., Sanchez, J-Y. & Armand, M. Electrochemical study of linear and crosslinked POE-based polymer electrolytes. *Electrochim. Acta* **37,** 1699–1701 (1992).

in a non-diffusing state in a static matrix. With increasing temperature, the onset of diffusive motions causes the linewidth to fall towards values characteristic of a fluid liquid. In a simple lithium compound, this line narrowing would take place just below the melting point. In contrast, two distinct steps as a function of increasing temperature are observed in Fig. 5. The higher-temperature step corresponds to the melting transition in P$_{12}$. The much larger line-narrowing event takes place around −20 °C and is complete by 0 °C, well below the melting point of the compound. The diffusive motions causing line narrowing could involve the lithium ion itself or its immediate neighbours. Line narrowing therefore does not offer conclusive proof of lithium ion motion below the melting point. However, in combination with the observation that the addition of the lithium ion dopant, along with an anion which is common to the matrix, produces a 50-fold increase in conductivity without altering the phase behaviour of the material, it appears likely that it is lithium ion motion which is responsible for both the NMR line narrowing and the increased conductivity. Conduction thus being substantially due to the Li$^+$ ion alone is in stark contrast to polymer electrolyte materials in which lithium ion motion makes up only a small (<20%) fraction of the ion conductivity[2].

The doped P$_{1x}$ materials we report here can be classified as fast ion conductors on the basis of the high conductivities observed in a crystalline lattice. These crystalline materials have plastic mechanical properties at room temperature; that is, at some value of applied stress the materials will yield and exhibit plastic flow. Both the flow and the fast ion conduction properties are a result of rotational disorder and the existence of vacancies in the lattice. The materials therefore express an important decoupling of various molecular motions from one another such that an unusual combination of properties is exhibited. NMR relaxation measurements in progress should determine the various motional timescales that are present in these materials. □

1. Gray, F. M. *Solid Polymer Electrolytes: Fundamentals and Technological Applications* 13 (VCH, New York, 1991).
2. Ma, Y. *et al.* The measurement of a complete set of transport properties for a concentrated solid polymer electrolyte solution. *J. Electrochem. Soc.* **142,** 1859–1868 (1995).
3. Doeff, M. M., Ferry, A., Ma, Y., Ding, L. & De Jonghe, L. C. Effect of electrolyte composition on the performance of sodium/polymer cells. *J. Electrochem. Soc.* **144,** L20–L22 (1997).
4. Wong, S. *et al.* Towards elucidating microscopic structural changes in Li-ion conductors Li$_{(1+y)}$Ti$_{(2−y)}$Al$_y$(PO$_4$)$_3$ and Li$_{1+y}$Ti$_{2+y}$Al(PO$_4$)$_{3−x}$(MO$_4$)$_x$ (M = V and Nb): x-ray and ^{27}Al and ^{31}P NMR studies. *J. Mater. Chem.* **8,** 2199–2203 (1998).
5. Adachi, G-Y., Imanaka, N. & Aono, H. Fast Li$^+$ conducting ceramic electrolytes. *Adv. Mater.* **8,** 127–134 (1996).
6. Timmermans, J. Plastic crystals: a historical review. *J. Phys. Chem. Solids* **18,** 1–8 (1961).
7. Handra, D., Helmes, J. H. & Majumdar, A. Ionic conductivity in ordered and disordered phases of plastic crystals. *J. Electrochem. Soc.* **141,** 1921–1927 (1994).

······································

Patterning liquid flow on the microscopic scale

Dawn E. Kataoka & Sandra M. Troian

Department of Chemical Engineering, Princeton University, Princeton, New Jersey 08544-5263, USA

····································

Microscopic fluidic devices, ranging from surgical endoscopes[1] and microelectromechanical systems[2] to the commercial 'lab-on-a-chip' (ref. 29), allow chemical analysis and synthesis on scales unimaginable a decade ago. These devices transport miniscule quantities of liquid along networked channels. Several techniques have been developed to control small-scale flow, including micromechanical[3] and electrohydrodynamic[4] pumping, electro-osmotic flow[5], electrowetting[6,7] and thermocapillary pumping[8–10]. Most of these schemes require micro-machining of interior channels and kilovolt sources to drive electrokinetic flow. Recent work[8–10] has suggested the use of temperature instead of electric fields to derive droplet movement. Here we demonstrate a simple, alternative technique utilizing temperature gradients to direct microscopic flow on a selectively patterned surface (consisting of alternating stripes of bare and coated SiO$_2$). The liquid is manipulated by simultaneously applying a shear stress at the air–liquid interface and a variable surface energy pattern at the liquid–solid interface. To further this technology, we provide a theoretical estimate of the smallest feature size attainable with this technique.

A thin, wetting film in contact with a solid substrate bearing a temperature gradient will flow from warmer to cooler regions because of the development of a thermocapillary shear stress at the air–liquid interface[11]. For sufficiently thin films in which the thermal conductive resistance is much smaller than the convective resistance (that is, at small Biot number), the applied thermal gradient at the solid surface is directly transferred to the air–liquid interface. Because most liquids maintain a negative and constant value of dγ/dT, where γ is the surface tension and T is the temperature, the application of a constant thermal gradient in
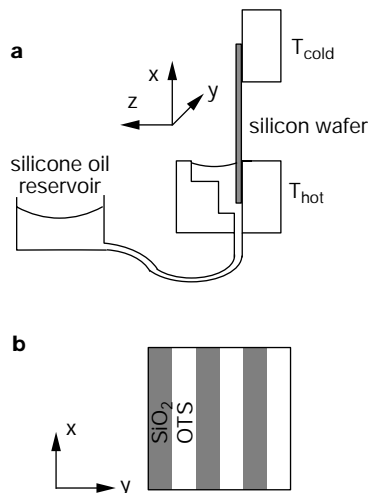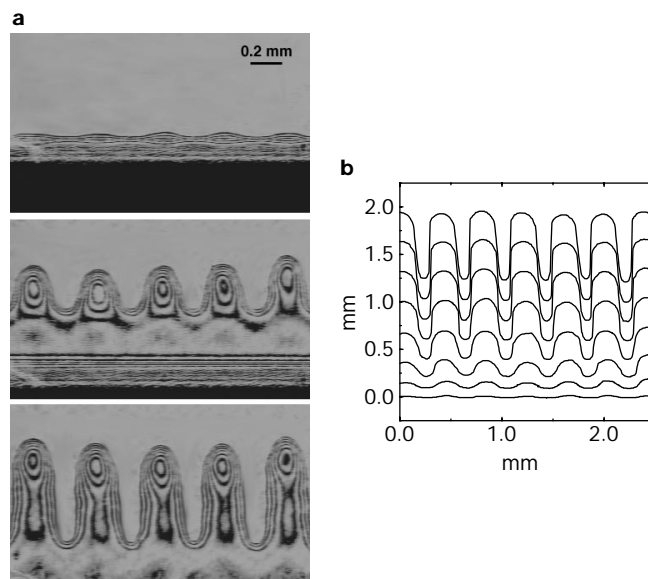
Figure 1 Schematic diagrams of the experimental apparatus (**a**) and the orientation of the patterned Si wafer (**b**). The wafer was patterned by spin-coating photoresist onto an OTS-coated wafer for 40 s at 4,000 r.p.m., and baking for 20 min at 90 °C. Using a mask aligner, the wafer was then exposed to UV light through a mask consisting of vertical stripes. The wafer was placed in a developer which stripped away the exposed photoresist, baked at 90 °C for 20 min, then subjected to an oxygen plasma for 20 s; the plasma removed any remaining OTS which lay beneath the developed photoresist. The wafer surface now consisted of alternating stripes of bare, oxidized SiO_2 and photoresist-covered OTS. A final acetone rinse removed the undeveloped photoresist, leaving the OTS monolayer intact. Contact angle measurements with water on surfaces patterned at a larger scale indicated that the uncoated silicon portions were completely hydrophilic, while the OTS-coated portions produced an angle >110°, as required for uniform OTS monolayers[26,27].

Figure 2 Time series of a silicone-oil film spreading on a patterned silicon wafer. The pattern consists of alternating 200-μm-wide stripes of OTS and bare oxidized SiO_2, and the spreading was monitored by interferometry. **a**, Three interferograms, with a five minute lapse between each. Adjacent fringes correspond to a change in film thickness of 0.2255 μm. **b**, A series of digitized curves, with a two minute lapse between each, representing the liquid front. The applied shear stress for **a** and **b** is $\tau = 0.8$ dyn cm^{-2}.

the streaming ($\hat{x}$) direction produces a fixed shear stress at the air–liquid surface given by $\tau = d\gamma/dx = (d\gamma/dT)(dT/dx)$. Films that are driven by a thermocapillary shear stress can even climb a vertical substrate, provided that the upward flux due to thermal stresses is larger than the downward flux due to gravitational drainage (that is, $h_0 \ll 3\tau/2\rho g$, where h_0 is the film thickness, ρ is the fluid density and g is the gravitational acceleration). In systems with large surface-to-volume ratio, as in microscale flows, even small thermal gradients can produce significant liquid movement.

Thermocapillary spreading on homogeneous surfaces has been shown to undergo a hydrodynamic instability for sufficiently thin films or large surface stress[12–16]. In this limit, the spreading front develops a thickened capillary ridge; for a certain range of transverse wavenumbers, this ridge becomes unstable to the formation of numerous, parallel rivulets whose spacing is governed by a characteristic wavelength, $\lambda_c \propto h_0(3Ca)^{-1/3}$. The capillary number, $Ca = \eta V/\gamma$, represents the balance between the viscous, capillary and thermocapillary force where η is the liquid viscosity and V is the steady-state spreading velocity. For films driven by this thermocapillary effect[14], $Ca = \tau h_o/2\gamma$ and $\lambda_c = 18(2\gamma h_o^2/3\tau)^{1/3}$. Energy decomposition techniques have identified the source of instability[14–16]: disturbances which cause a local protrusion in the spreading front create thickened portions which spread faster than adjacent thinner regions, thereby destabilizing an initially uniform front. This same mechanism, first described by Spaid and Homsy[17], is responsible for the fingering instability observed in gravitational[18–22] and centrifugal[17,23,24] flows.

From a technological point of view, the possibility of using this spontaneous pattern formation to channel microvolumes of liquid along a substrate is questionable. For spreading on homogeneous surfaces, the rivulets almost never appear in the same position along the spreading front. In addition, surface defects or contaminant particles tend to produce flow irregularities which create as much as
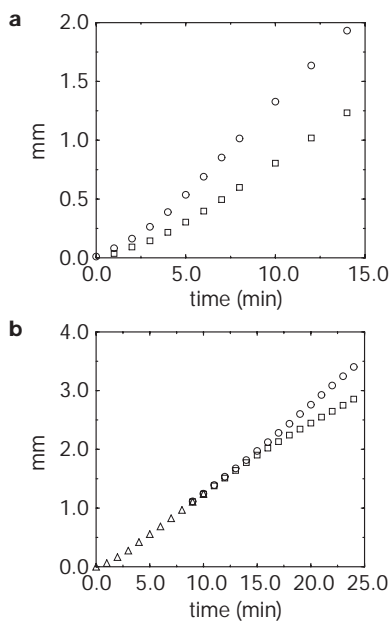
a 30% variation in the natural wavelength, λ_c (refs 21, 22, 25). There exists, however, a special feature of thermally driven films which can be manipulated to regularize the flow along selected, prescribed lanes. Even small thermal gradients produce liquid films less than a micrometre in thickness[12,13,25]. These films therefore maintain an excessively large surface to volume ratio. The combination of an applied shear stress at the air–liquid surface and a patterned surface energy profile at the liquid–solid interface can be used to direct microscale flow along prescribed lanes. The flows produced in this manner are stable and reproducible, as the surface patterns control accessible or non-accessible regions. Because of the strong influence of the solid surface, the flow also rapidly self-corrects in the presence of defects or surface contaminants, always keeping perfect registry with the surface pattern. From a practical and fundamental point of view, it is therefore interesting to explore the consequences of patterning the surface with a wavelength different from the natural wavelength which would be selected by the liquid were it to spread on a homogeneous surface. Our results show that the instability wavelength can be easily superseded by the substrate pattern, provided that the width of the liquid channels exceeds a lower critical value.

We have examined the thermocapillary spreading of a silicone oil films (PDMS, both with viscosity of 18 mPa s and surface tension of 21 dyn cm^{-1} at 25 °C, Aldrich) on vertically oriented, patterned silicon wafers. The wafers were held vertical by suction against two brass blocks maintained at different temperatures by two circulating baths (see Fig. 1a). The thermal gradient was recorded after each experimental run by six equally spaced, fine wire thermocouples (0.005 inch diameter, copper/constantin, Omega). For the temperature range we studied, silicone oil maintains a value of $d\gamma/dT = -0.05$ dyn cm^{-1} °C^{-1}. When placed in contact with the heated portion of the substrate, the silicone oil spontaneously climbs along the wafer surface. The brass block at the higher temperature was fed by a small Teflon tube connected to a reservoir of silicone oil mounted on a vertical stage (Fig. 1a). By varying the height of the stage, the meniscus level on the wafer could be adjusted precisely. In these experiments, the shear stress, τ, was in the range 0.73–0.80 ($\pm$10%) dyn cm^{-2}.

The surface pattern chosen for study was a sequence of alternating vertical stripes whose wavelength ranged from 50 to 500 μm. The vertical stripes consisted either of bare, naturally oxidized silicon (SiO_2), or oxidized silicon coated with a covalently bonded monolayer of octadecyltrichlorosilane (OTS). The orientation of the patterned wafer is shown in Fig. 1b. The wafers were cleaned, and then immersed in an OTS solution under a nitrogen atmosphere, according to published procedures[26]. OTS monolayers prepared by this method have been shown to produce a stable and complete monolayer of 26 Å thickness[27]. The coated wafers were then patterned by photolithography as described in Fig. 1 legend. This same procedure works equally well on glass substrates. We also tried patterning the OTS monolayer using deep ultraviolet (193 nm) illumination through a fused silica mask[28]; this one-step procedure also produced excellent results.

The topography of the spreading film was visualized by laser interferometry. Light from a He–Ne laser (wavelength 6,328 Å) impinged on the substrate at normal incidence, producing the interferograms shown in Fig. 2a. The interfringe spacing corresponds to a change in film thickness of 0.2555 μm. Typical film thicknesses were less than 1 μm for these shear stresses. The images were used to monitor the speed of the advancing front, and to reconstruct the entire surface shape. The images were recorded with a high-resolution CCD camera (MTI VE1000, Dage) fitted with a Navitar zoom lens and stored on SVHS tapes for image analysis. Further details can be found in ref. 25.

We first examined the spreading behaviour of silicone oil on homogeneous surfaces consisting either of bare, oxidized SiO_2 wafers, or wafers fully coated with OTS. Contact angle and work of adhesion measurements for silicone oil on either substrate revealed a very small and similar contact angle. (According to Young's equation, however, this does not imply that the liquid–solid surface energy is the same.) The spreading on either homogeneous surface proceeded by the instability mechanism described earlier, with a well defined natural wavelength set by λ_c. The spreading velocities were also similar.

Experiments with the patterned wafers revealed a very different flow behaviour. Figure 2a shows a time sequence of the liquid film spreading on a wafer bearing alternating 200-μm-wide stripes of OTS and uncoated SiO_2. Whereas (unstable) rivulet formation on homogeneous surfaces always requires an incubation period during which the front spreads as a straight line before fingering, the flow on patterned surfaces is immediately channelled into well defined lanes whose spacing is imposed by the surface pattern (Fig. 2b). In Fig. 3, we have plotted the advance of the spreading front on a patterned and homogeneous substrate (bare SiO_2) with all other variables remaining constant. The spreading on the patterned wafers (Fig. 3a) immediately creates alternating tips (circles) and troughs (squares). The homogeneous surface instead allows uniform spreading for over 15 min before the front becomes unstable (Fig. 3b), spontaneously splitting into tips (circles) and troughs (squares). For a shear stress $\tau = 0.8\,\mathrm{dyn\,cm^{-2}}$, the average speed of the tips and troughs on the patterned wafer was $2.60\,\mathrm{\mu m\,s^{-1}}$ and $1.73\,\mathrm{\mu m\,s^{-1}}$ and on the bare wafer $2.56\,\mathrm{\mu m\,s^{-1}}$ and $1.94\,\mathrm{\mu m\,s^{-1}}$, respectively. The tips advanced at similar speed on either surface, while the troughs appeared to advance more slowly on the OTS segments.

In Table 1 we summarize the results for spreading on homogeneous and patterned surfaces with variable width strips. In all cases, the silicone oil preferentially spread on the uncoated SiO_2 portions. This is not surprising, as a clean silicon wafer covered by natural oxide layer has a high surface energy and therefore a high affinity for water and organic contaminants. Organic monolayers terminating in methyl and vinyl groups have low surface energy, and resist organic contamination[27]. For the homogeneous surfaces, the periodicity agrees well with the predicted value for λ_c. On the patterned surfaces, the periodicity of the spreading front, λ_{exp}, agrees well with the periodicity imposed by the solid substrate, λ_{solid}. The excellent registry with the imposed surface pattern persisted for all flows except the last entry. In this last example, the liquid was unable to follow the narrow surface lanes and reverted back to the natural wavelength that would be obtained on a homogeneous surface.

A simple scaling argument predicts the approximate lane width for which the capillary pressure at the tip of a liquid channel is strong enough to oppose the upward thermally driven flow for patterned spreading. In this limit, the upward volumetric flux, $\tau h_0^2/2\eta$, is opposed by the downward capillary flux, $h_0^3(\mathrm{d}p/\mathrm{d}x)/3\eta$, where p is the Laplace pressure. For a completely wetting liquid, $(\nabla h_0)^2 \ll 1$, $\mathrm{d}p/\mathrm{d}x \sim O(\gamma h_0/R^3)$, where R denotes the radius of curvature in the streaming direction. This balance produces a lower critical value of $R \sim (\gamma h_0^2/\tau)^{1/3}$. Strong curvature in the transverse ($\hat{y}$) direction, which induces lateral flow, can also force liquid to spread over the OTS stripes. However, without an estimate for the pinning force exerted by the junction between the OTS and uncoated stripes, the corresponding force balance cannot be expressed. Nonetheless, as seen in Fig. 2, the radius of curvature

Figure 3 Comparison between the location of the liquid front for spreading on a patterned and an homogeneous surface. Circles and squares represent liquid channel tips and troughs, respectively. **a**, Silicone oil spreading on a wafer patterned with alternating 200-μm-wide stripes of OTS and bare oxidized SiO_2. **b**, Silicone oil spreading on a homogeneous, bare, oxidized SiO_2 wafer. The applied shear stress in **a** and **b** is $\tau = 0.8\,\mathrm{dyn\,cm^{-2}}$.

Table 1 Liquid lane spacing for silicone oil spreading on homogeneous and patterned surfaces

τ (dyn cm^{-2})	W_{OTS} (μm)	W_{SiO_2} (μm)	λ_{solid} (μm)	λ_{exp} (μm)
0.79	–	All	–	574
0.79	All	–	–	545
0.77	250	250	500	489
0.80	200	200	400	399
0.76	150	150	300	288
0.73	250	150	400	393
0.73	150	250	400	394
0.74	50	50	100	545

The first two rows show data for fully uncoated and coated surfaces, respectively. τ is the applied surface stress, W_{OTS} and W_{SiO_2} denote the widths of each type of lane, $\lambda_{solid} = W_{OTS} + W_{SiO_2}$ denotes the wavelength of the repeating surface pattern, and λ_{exp} represents the average measured distance between adjacent finger tips. The distance, λ_{exp}, was obtained from an edge-detection algorithm which averaged over 10–20 liquid fingers.

in both the streaming and transverse direction is fairly similar, so that this estimate for R provides a reliable lower cut-off. This critical value can be made even smaller by decreasing γ (using different liquids or introducing surfactants), and by decreasing h_0 or increasing τ. Typical values for the film thickness (1 μm), surface tension (20 dyn cm^{-1}), and shear stress (1 dyn cm^{-2}) yields a characteristic finger or lane width, $2R \sim O(100\,\mu m)$, in good agreement with the flow behaviour observed in the last entry of Table 1.

To develop further this technology for microfluidic applications, the troughs of the liquid front can be pinned in place, allowing liquid to flow only along specified surface lanes. This can be accomplished by either decreasing the surface energy of adjacent lanes (so that the liquid becomes partially or even non-wetting along those stripes) or by micromachining flow obstacles at the liquid entrance point. We are experimenting with different mono-layer treatments for this purpose. We have also patterned more complicated surface networks to force liquid to spread in curved lanes and around corners by the application of thermal gradients in and across the streaming direction. In this way, we can achieve precise flow control at the microscopic scale by simultaneously manipulating the boundary conditions at the air–liquid and liquid–solid interfaces. These concepts should be generalizable to other driving forces which are proportional to the surface area of the fluid, not to its volume. □

1. Menz, W. & Guber, A. Microstructure technologies and their potential in medical applications. *Min. Invasive Neurosurgery* **37,** 21–27 (1994).
2. Ho, C. H. & Tai, Y. C. Micro-electro-mechanical-systems (MEMS) and fluid flows. *Annu. Rev. Fluid Mech.* **30,** 579–612 (1998).
3. van Lintel, H. T. G. A piezoelectric micropump based on micromachining of silicon. *Sensors Actuators* **15,** 153–167 (1988).
4. Bart, S. F., Tarrow, L. S., Mehregany, M. & Lang, J. H. Microfabricated electrohydrodynamic pumps. *Sensors Actuators A* **21–23,** 193–197 (1990).
5. Manz, A. *et al.* Electroosmotic pumping and electrophoretic separations for miniaturized chemical analysis systems. *J. Micromech. Microeng.* **4,** 257–265 (1995).
6. Beni, G. & Tenan, M. A. Dynamics of electrowetting displays. *J. Appl. Phys.* **52,** 6011–6015 (1981).
7. Gallardo, B. S. *et al.* Electrochemical principles for active control of liquids on submillimeter scales. *Science* **283,** 57–89 (1999).
8. Handique, K., Gogoi, B. P., Burke, D. T., Mastrangelo, C. H. & Burns, M. A. Microfluidic flow control using selective hydrophobic patterning. *Proc. SPIE* **3224,** 185–195 (1997).
9. Handique, K., Burke, D. T., Gogoi, B. P., Mastrangelo, C. H. & Burns, M. A. in *Technical Digest: Solid State Sensor and Activator Workshop* 346–349 (Transducer Research Foundation, Cleveland, Ohio, 1998).
10. Sammarco, T. S. & Burns, M. A. Thermocapillary pumping of discrete drops in microfabricated analysis devices. *Am. Inst. Chem. Eng. J.* **45,** 350–366 (1999).
11. Ludviksson, V. & Lightfoot, E. N. The dynamics of thin liquid films in the presence of surface-tension gradients. *Am. Inst. Chem. Eng. J.* **17,** 1166–1173 (1971).
12. Cazabat, A. M., Heslot, F., Troian, S. M. & Carles, P. Fingering instability of thin spreading films driven by temperature gradients. *Nature* **346,** 824–826 (1990).
13. Brzoska, J. B., Brochard-Wyart, F. & Rondelez, F. Exponential growth of fingering instabilities of spreading films under horizontal thermal gradients. *Europhys. Lett.* **19,** 97–102 (1992).
14. Kataoka, D. E. & Troian, S. M. A theoretical study of instabilities at the advancing front of thermally driven coating films. *J. Colloid Interface Sci.* **192,** 350–362 (1997).
15. Kataoka, D. E. & Troian, S. M. Stabilizing the advancing front of thermally driven coating films. *J. Colloid Interface Sci.* **203,** 335–344 (1998).
16. Kataoka, D. E. & Troian, S. M. The transient dynamics and structure of optimal excitations in thermally driven films. *Phys. Fluids.* (submitted).
17. Spaid, M. A. & Homsy, G. M. Stability of Newtonian and viscoelastic dynamic contact lines. *Phys. Fluids* **8,** 460–478 (1996).
18. Huppert, H. E. Flow and instability of a viscous current down a slope. *Nature* **300,** 427–429 (1982).
19. Silvi, N. & Dussan, E. B. On the rewetting of an inclined solid surface by a liquid. *Phys. Fluids* **28,** 5–7 (1985).
20. Troian, S. M., Herbolzheimer, E., Safran, S. A. & Joanny, J. F. Fingering instabilities of driven spreading films. *Europhys. Lett.* **10,** 25–30 (1989).
21. Jerrett, J. M. & deBruyn, J. R. Finger instability of a gravitationally driven contact line. *Phys. Fluids A* **4,** 234–242 (1992).
22. deBruyn, J. R. Growth of fingers at a driven three phase contact line. *Phys. Rev. A* **46,** R4500–R4503 (1992).
23. Melo, F., Joanny, J. F. & Fauve, S. Fingering instability of spinning drops. *Phys. Rev. Lett.* **63,** 1958–1961 (1989).
24. Fraysse, N. & Homsy, G. M. An experimental study of rivulet instabilities in centrifugal spin coating of viscous Newtonian and non-Newtonian fluids. *Phys. Fluids* **6,** 1491–1504 (1994).
25. Kataoka, D. E. *The Spreading Behavior of Thermally Driven Liquid Films.* Thesis, Princeton Univ. (1999).
26. Brzoska, J. B., Ben Azouz, I. & Rondelez, F. Silanization of solid substrates: a step toward reproducibility. *Langmuir* **10,** 4367–4373 (1994).
27. Wasserman, S. R. *et al.* The structure of self-assembled monolayers of alkylsiloxanes on silicon: a comparison of results from ellipsometry and low-angle x-ray reflectivity. *J. Am. Chem. Soc.* **111,** 5852–5861 (1989).
28. Dulcey, C. L. *et al.* Deep UV photochemistry of chemisorbed monolayers: patterned coplanar molecular assemblies. *Science* **252,** 551–554 (1991).
29. Freemantle, M. Downsizing chemistry *Chem. Eng. News* **77(8),** 27–36 (1999).

Stabilizing a solid–solid interface with a molecular-scale adhesive

R. J. Davey, L. Williams-Seton, H. F. Lieberman & N. Blagden

Colloids, Crystals and Interfaces Group, Department of Chemical Engineering, UMIST, Manchester M60 1QD, UK

The industrial importance of molecular materials chemistry has promoted great interest in areas such as self-assembled surface coatings[1], multi-layer formation on solid substrates[2], crystallization from solutions[3], crystal morphology[4] and structure prediction[5], solving structures from powders[6] and control of polymorphism[7]. Improvements in our understanding of the role of intermolecular interactions in driving molecular self-assembly and interfacial processes have led to technological advances— both in controlling the assembly of molecules at the nanometre scale, and in manipulating processes and products in which crystal nucleation and growth are key elements[8]. But there has been relatively little work on molecular-scale engineering at solid–solid interfaces, despite their importance in polymeric
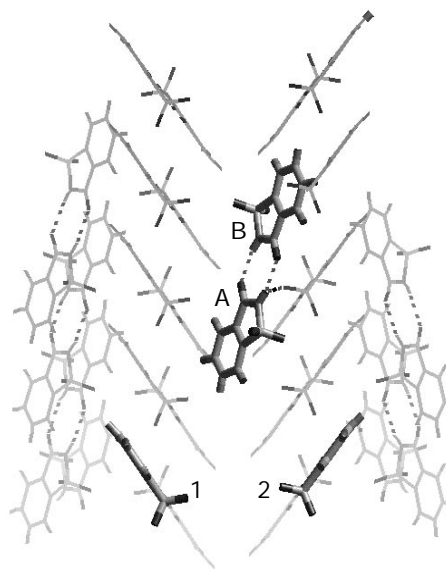
Figure 1 The (10$\bar{2}$) twin interface in saccharin viewed normal to (10$\bar{2}$). Molecules A and B, lying in the twin plane, illustrate how the structure is created from hydrogen-bonded dimers. Molecules 1 and 2, appearing side on, are related across the twin interface by mirror symmetry.